PHYSICAL REVIEW D **78,** 114503 (2008)

QCD at finite chemical potential with six time slices

R. V. Gavai* and Sourendu Gupta†

Department of Theoretical Physics, Tata Institute of Fundamental Research, Homi Bhabha Road, Mumbai 400005, India

(Received 10 July 2008; revised manuscript received 21 October 2008; published 15 December 2008)

We investigate the Taylor expansion of the baryon number susceptibility, and hence, pressure, in a series in the baryon chemical potential (μ_B) through a lattice simulation with two flavors of light dynamical staggered quarks at a finer lattice cutoff $a = 1/6T$. We determine the QCD cross over coupling at $\mu_B = 0$. We find the radius of convergence of the series at various temperatures, and bound the location of the QCD critical point to be $T^E/T_c \approx 0.94$ and $\mu_B^E/T < 1.8$. We also investigate the extrapolation of various susceptibilities and linkages to finite chemical potential.

DOI: 10.1103/PhysRevD.78.114503 PACS numbers: 12.38.Aw, 05.70.Fh, 11.15.Ha

I. INTRODUCTION

In the near future experiments at the Relativistic Heavy-Ion Collider (RHIC) in Brookhaven [1] will begin to search for the critical end point of QCD [2], and in the process also study other physics at finite chemical potential. In this paper we present an improvement on previous lattice results at finite chemical potential μ and temperature T by decreasing the lattice spacing to $a = 1/6T$ while working, as before, in QCD with two flavors of light dynamical staggered quarks. We investigate the physics at finite μ using the method of Taylor expansions that was developed in [3] and used for QCD earlier with $a = 1/4T$ [4,5]. One of the quantities we investigate is the radius of convergence of the Taylor series, through which we estimate the QCD critical point. We also investigate the dependence on μ of various other quantities of physical interest. Finally, we investigate the linkage of quantum numbers and its dependence on T and μ. Related earlier works all used $a = 1/4T$, but different methods or inclusion of μ and different numbers of flavors [6].

That phase transitions are rounded off by finite-size effects was discovered long ago by van Hove. The most familiar aspects are seen when simulations are directly performed in the vicinity of the critical coupling. Quantities which would diverge in the thermodynamic (infinite volume) limit are finite. As a result, a lattice computation never sees a singularity, but infers its existence from some measures. Proofs of the existence usually involve testing extrapolations: such are the main remaining problems at finite temperature and vanishing chemical potential. A well-developed finite-size scaling theory can be used to study the size L dependence of such quantities and extract critical exponents. To date, the immensity of computational requirements has prevented full use of this theory for QCD.

The study of the effect of the finite-size rounding of critical points on series expansions is, to the contrary, in its infancy. The clearest fact about such effects is the following: since quantities which should diverge in the thermodynamic limit merely have finite peaks at finite L, series expansions, strictly speaking, have finite radii of convergence for finite L. In the limit $L \to \infty$ the radius of convergence estimates the nearest critical point. The mechanism by which this limit is reached is straightforward. Were one to examine some estimator of the radius of convergence at order n, $R_n(L)$, one would find that up to some $n \leq n_*(L)$ the $R_n(L)$ would approach a finite value. Such behavior was exhibited for the series expansion in QCD in Fig. 16 of [4]. For larger n the R_n would diverge, in accordance with van Hove's theorem. With increasing L one would find that $n_*(L)$ approaches infinity (see Fig. 1). How the scaling of $n_*(L)$ with L codes for the critical exponent is presently unknown.

Another question that can be answered by the series expansion is where the singularity lies. In the case of QCD, the question is whether the finite radius of convergence of the series expansion in μ is due to a singularity at real μ. If it is, then the successive coefficients in the expansion are positive. At finite L one must examine the

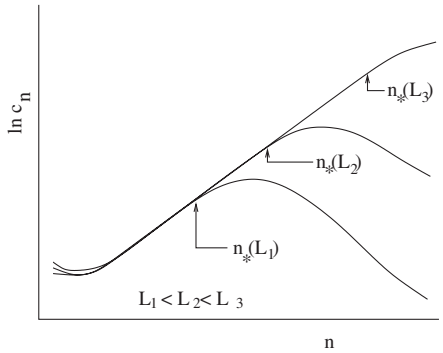

FIG. 1. Series coefficients $c_n(L)$ for a quantity that diverges in the thermodynamic limit, $L \to \infty$, at the critical point have the finite-size behavior shown here. The radius of convergence, $R_n = c_{n-1}/c_n$, plateaus for $n < n_*(L)$ before rising to infinity. The case shown here corresponds to a singularity on the real axis, since all the c_n in the plateau are positive.

*gavai@tifr.res.in
†sgupta@tifr.res.in

signs of the series coefficients for $n < n_*(L)$. If these are positive, then the singularity which limits the expansion when $L \to \infty$ is on the real axis. In [4] this argument was used to justify the identification of the radius of convergence with the critical point. This argument is also implicit in [7].

In summary, the quark number susceptibilities are Taylor coefficients in the expansion of the pressure in powers of the chemical potential. From the series expansion for the pressure,

$$P(T, \mu_B) = P(T) + \frac{1}{2}\chi_B^{(2)}(T)\mu_B^2 + \frac{1}{4!}\chi_B^{(4)}(T)\mu_B^4 + \frac{1}{6!}\chi_B^{(6)}(T)\mu_B^6 + \frac{1}{8!}\chi_B^{(8)}(T)\mu_B^8 + \cdots, \quad (1)$$

we define the nonlinear susceptibilities (NLS) of the nth order, $\chi_B^{(n)}$. The second order susceptibility, also called the quark number susceptibility (QNS) [8], has the expansion

$$\chi_B(T, \mu_B) = \chi_B^{(2)}(T) + \frac{1}{2}\chi_B^{(4)}(T)\mu_B^2 + \frac{1}{4!}\chi_B^{(6)}(T)\mu_B^4 + \frac{1}{6!}\chi_B^{(8)}(T)\mu_B^6 + \cdots. \quad (2)$$

This series is expected to diverge at the QCD critical end point. Estimators of the radius of convergence of this series are

$$\mu_*^{(n)} = \sqrt{n(n+1)\frac{\chi_B^{(n+1)}}{\chi_B^{(n+3)}}}, \quad \text{or} \quad \bar{\mu}_*^{(n)} = \left(n!\frac{\chi_B^{(2)}}{\chi_B^{(n+2)}}\right)^{1/n}. \quad (3)$$

When successive estimators are equal within statistical errors to the same value μ_*, we have identified the plateau in the radius of convergence. This corresponds to the critical point, provided the singularity in the series occurs at a real value of μ_*. In turn, this is the case when the coefficients from which the estimates are made are all positive.

In the next section we present the details of the simulation and the extraction of the critical coupling. This is followed by a section in which we report the main results, namely, the extraction of the QNS up to the eighth order. This results in five terms of the series for the pressure, and four terms of the series for the baryon number susceptibility. Using these we report our result for the radius of convergence of the series, and extract from this our best estimate of the critical point. In the section after this we discuss the extrapolation of physical quantities to large chemical potentials. This extrapolation throws more light on the nature of the QCD critical point.

Note that the series in Eqs. (1) and (2) cannot be continued beyond μ_* even when all the terms are known exactly. The truncated series expansion fails even faster. As a result, it becomes difficult to extrapolate physical quantities to large values of μ_B. One way to use the series to a better advantage is well known: the method of Padé approximants. The existing theory of Padé approximants [9] is adapted to the case where each known series coefficient has infinite numerical accuracy. When coefficients are extracted through Monte Carlo estimates, and hence have statistical errors, new issues arise. We believe that it would be useful to extend the theory of Padé approximants in this direction. In the appendix we make a beginning which is adequate for the purpose of this paper.

II. SIMULATIONS

The simulations were performed (see Table I) using the R-algorithm for hybrid molecular dynamics. This uses a finite step size, δt, for the molecular dynamics (MD). Our main data set is generated using $\delta t = 0.01$ and a total trajectory length of $t = 1$ in MD time units. We performed tests of the accuracy and efficiency of the choices.

Most of our computations were performed with $\delta t = 0.01$. This was found to be adequate for computations at $N_t = 4$. We checked our results at $T/T_c = 1.00$ by running a long computation with $\delta t = 0.001$ and trajectory length of 3 MD time units. We found complete agreement between the runs with two different time steps. In Table II we show the comparison of bulk quantities computed in the two runs.

Changing the trajectory length from $t = 1$ to $t = 3$ at $T/T_c = 0.94 \pm 0.01$, 1.00 ± 0.01, and 1.92 ± 0.05 did not change the results for thermodynamic quantities within errors. However, near T_c the longer trajectories were more effective at reducing the autocorrelation time. For example, we found that the longest autocorrelation time at β_c was $\tau_{\rm int} \approx 267$ trajectories for $T = 1$, and it reduced to 36 for $t = 3$. As a result, the CPU time taken to produce decorrelated configurations is reduced by a factor of about 2.5 on taking the longer trajectories. At $T/T_c = 0.94 \pm 0.01$ the effective speedup, computed in the same way, was a little under a factor of 2. In the high-temperature phase the autocorrelation times were very small, and there was little to be gained by using longer molecular dynamics trajectories. There were no changes in thermodynamic quantities on changing the trajectory length.

A range of β was scanned, as indicated in Table I, to locate the bare coupling at the finite temperature crossover β_c. The crossover was located by the peak of the unrenormalized Polyakov loop susceptibility,

$$\chi_L = N_s^3(\langle L^2\rangle - \langle L\rangle^2), \quad \text{where } L = \frac{1}{3N_s^3}\sum_x \mathrm{Re}\,\mathrm{Tr}P(x) \quad \text{and} \quad P(x) = \prod_{t=1}^{N_t} U_{\hat{t}}(x, t). \quad (4)$$

Here $U_{\hat{t}}(x, t)$ is the gauge link in the time direction at the spatial site x on the time slice t. We shall show later that the fourth order quark number susceptibility also peaks at the

TABLE I. The simulation parameters. These simulations used the R-algorithm with a step size of $\delta T_{MD} = 0.01$ and a trajectory length of $T_{MD} = 1$. For tests of accuracy, see later.

β	m_b/T_c	T/T_c	6×12^3		6×18^3		6×24^3	
			N_t	τ_{int}	N_t	τ_{int}	N_t	τ_{int}
5.39	0.092 ± 0.005	0.89 ± 0.01					2284	33
5.40	0.100 ± 0.003	0.92 ± 0.01	22 599	88	10 099	48	919	35
5.41	0.094 ± 0.003	0.94 ± 0.01	50 584	197			14 580	131
5.415	0.097 ± 0.001	0.97 ± 0.01			17 518	179	14 044	158
5.42	0.099 ± 0.001	0.99 ± 0.01	39 649	164	35 649	165	27 974	140
5.425	0.1	1.00 ± 0.01	50 589	189	47 329	214	53 563	267
5.43		1.012 ± 0.001	54 619	218	41 349	147	41 869	202
5.46	0.11 ± 0.01	1.21 ± 0.01	309	13	10 719	13	1214	13
5.54	0.10 ± 0.01	1.33 ± 0.01					969	7
5.60	0.10 ± 0.03	1.48 ± 0.03					2891	4
5.75	0.10 ± 0.04	1.92 ± 0.05					3626	4

TABLE II. Comparison of bulk quantities, namely, the average and difference of spatial and temporal plaquette averages, the Wilson line, and the chiral condensate in runs with two different MD time steps for $\beta = 5.425$ on 6×24^3 lattices. In both cases the trajectory length was 3 MD time units and the first 1002 MD time units were discarded for thermalization. The number of trajectories used in the comparison was 2916 for the larger time step and 733 for the smaller time step.

Operator	$\delta t = 0.01$	$\delta t = 0.001$
$\langle P_s + P_t \rangle/2$	1.611(1)	1.611(2)
$10^4 \langle P_t - P_s \rangle$	7.8(4)	8.3(6)
$\langle \text{Re} L \rangle$	0.031(3)	0.032(6)
$\langle \bar{\psi} \psi \rangle$	0.293(9)	0.291(9)

same coupling. This is closely related to the inflection point of the second order susceptibility which is used by various groups [10].

From the peak of χ_L we identify $\beta_c = 5.425 \pm 0.005$ for $m/T_c = 0.1$, where the uncertainty is due to resolution, and not a statistical uncertainty. As expected, this is bracketed by results obtained with $m/T_c = 0.15$ [11] and 0.075 [12]. There is a little finite volume shift in the position of the peak of χ_L at the smallest volume, but no such shift is observed in going from $N_s = 18$ to $N_s = 24$ (see Fig. 2). While some volume dependence is visible in the peak of χ_L, with data from just these three volumes it is not possible to decide whether there is a crossover or a critical point at β_c. However, it is possible to rule out a first order transition, since $\chi_L^{\max}/N_s^3$ definitely drops with increasing N_s, as shown in Fig. 2.

Subsequently, $T = 0$ runs were performed on lattices of size 16^4 and 24^4 on a grid of β to determine the scale. The scale determination used the value of the plaquette to obtain the renormalized gauge coupling in the $\overline{\text{MS}}$ scheme. The errors in the scale setting involve the uncertainty in the

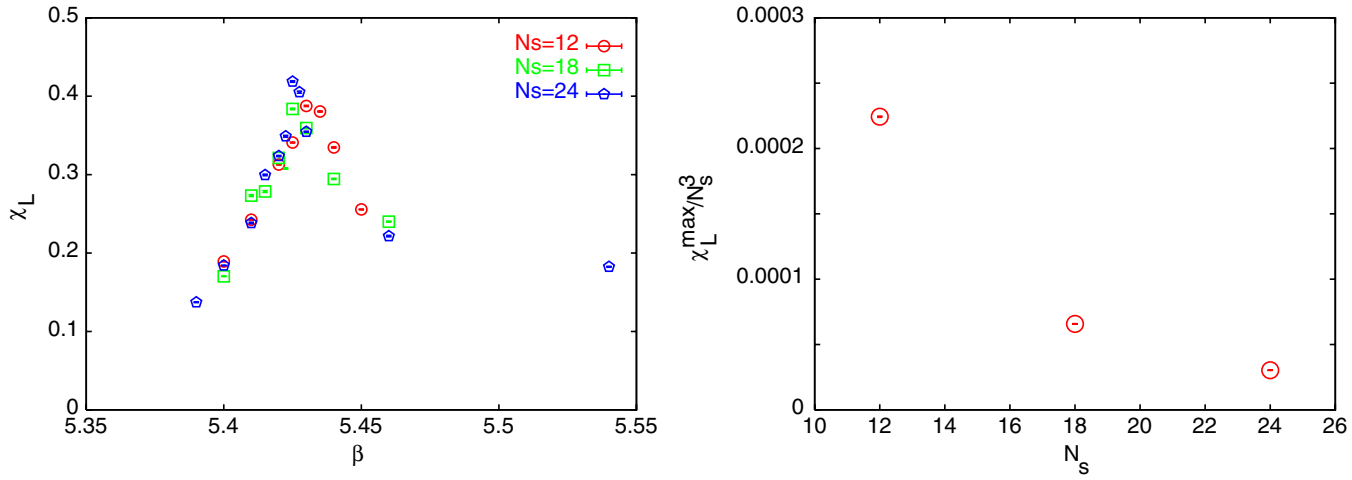

FIG. 2 (color online). The first figure shows χ_L as a function of β. There is some finite-size shift in the position of the peak at the lowest volumes. The second figure shows the volume dependence of the value of the peak, $\chi_L^{\max}$ as a function of N_s. It is clear that the peak grows slower than the volume N_s^3.

location of the crossover coupling β_c, statistical errors in plaquette measurements, and scheme dependence estimated by evaluating the scale also in the E and V schemes. In the range of temperatures within 20% of T_c, the largest errors came from the uncertainty in the determination of β_c. Better results can only be obtained by using larger spatial volumes. At larger temperatures, the scheme dependence of the scale set the largest errors. These can be reduced by going to smaller lattice spacing, i.e., to larger N_t. The scale setting using the crossover for $N_t = 6$ is compatible within errors with that obtained earlier for a similar setting of scales for $N_t = 4$ [4].

III. QUARK NUMBER SUSCEPTIBILITIES

A quick reminder of our notation [3,4] is in order. A quark number susceptibility is obtained by taking a derivative of the pressure with respect to the chemical potential. In two-flavor QCD there are two possible chemical potentials, μ_u and μ_d. If one takes j_u derivatives with respect to μ_u and j_d with μ_d, then the order of the quark number susceptibility is $n = j_u + j_d$. Since the u and d quarks are degenerate, and indistinguishable at $\mu_u = \mu_d = 0$, we denote the susceptibilities by $\chi_{j_u j_d}$ when $j_u > j_d$ and $\chi_{j_d j_u}$ when $j_d > j_u$. The susceptibilities are constructed from expectation values of a string of γ_0 operators sandwiched between quark propagators. The operator $\mathcal{O}_n$ is the operator with n insertions of γ_0 into a single fermion loop, and hence contributes only to χ_{n0}. The operators $\mathcal{O}_{abc\ldots}$ are products $\mathcal{O}_a\mathcal{O}_b\cdots$ and may contribute to several of the χ_{nm}. The construction of $\mathcal{O}_n$ on the lattice is given in detail in [4]. We shall discuss results for χ_{nm} as well as the expectation values $(T/V)\langle\mathcal{O}_{abc\ldots}\rangle$ (since we discuss only the connected pieces of these expectation values, we have not used a separate notation for that).

The quark number susceptibilities are obtained as expectation values of fermion loops with various operator insertions [4]. These are evaluated as usual through stochastic estimators. The computations were optimized using the methods of [4]. The need to use a large number of stochastic vectors has been discussed in detail elsewhere [13]. We have taken 500 random vectors for each trace evaluation. The necessity for such large numbers of vectors is clearly demonstrated in the data exhibited in Fig. 3.

With this we are able to control statistical errors on loops with up to six operator insertions. Even so, operators with larger numbers of loops remain noisy. Thus, at T_c on the largest volume, χ_{20} gives a signal at 53σ and χ_{40} at 23σ, whereas χ_{60} and χ_{80} give signals at 5σ and 3σ, respectively. For the two highest susceptibilities, this level of the signal is an improvement over the corresponding results with $N_t = 4$ at equal N_s/N_t. It was our experience at coarser lattice spacing that one needs lattices with larger spatial volumes to control loops with more insertions. We see this also at the current lattice spacings; at the smallest volumes, even loops with six insertions are hard to control.

In the following sections we will often compare results for $N_t = 4$ and $N_t = 6$. These results are meaningful only if they are done holding other factors fixed. We shall therefore compare the new results obtained on 6×24^3 lattices with those obtained earlier on 4×16^3 with the same quark mass, m/T_c.

A. Second order

The lowest order quark number susceptibilities are shown in Fig. 4. The diagonal susceptibility χ_{20} seems to show significant dependence on N_t, i.e., the lattice spacing. This is not a surprise; after all, even in the quenched theory a similar effect was seen [14]. The off-diagonal susceptibility χ_{11} seems to scale better with the lattice spacing.

Note that χ_{11} takes contributions only from $(T/V)\langle\mathcal{O}_{11}\rangle$, whereas χ_{20} has contributions from this as well as $(T/V) \times \langle\mathcal{O}_2\rangle$. The results shown in Fig. 4 indicate that the quark-

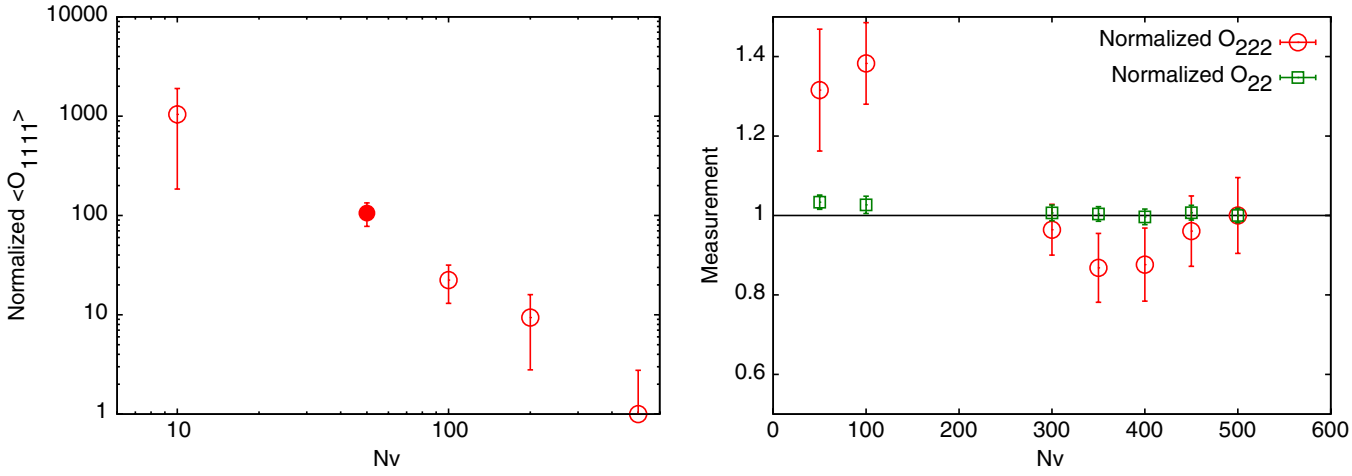

FIG. 3 (color online). The dependence of estimates for various multiloop operators on the number of stochastic vectors, N_v (all estimates are normalized to that obtained with $N_v = 500$). Note that the larger the number of loops, the larger are the number of vectors needed to control the result. For $\langle\mathcal{O}_{1111}\rangle$, the filled symbol denotes an estimate with the wrong sign.

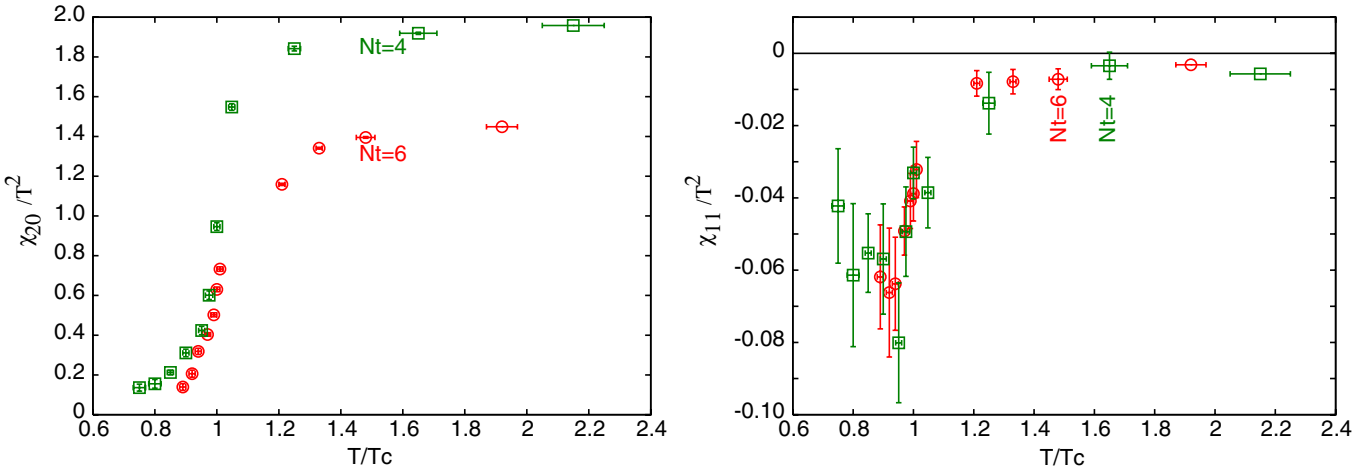

FIG. 4 (color online). The flavor diagonal and off-diagonal quark number susceptibilities on 6×24^3 (circles) and 4×16^4 (boxes) lattices.

line disconnected operator has, at best, marginal lattice spacing dependence. Most of the lattice spacing dependence seen in χ_{20} therefore comes from $(T/V)\langle \mathcal{O}_2 \rangle$. This last expectation value is the response to a chemical potential on the isospin component I_3 and hence was called χ_3 in some of our early papers. Both this and χ_{20} change rapidly near T_c and the "inflection point," i.e. the point at which the slope is maximum can be used as a corroborative measure of β_c. Because of the numerical uncertainties in taking derivatives of noisy data, we will instead use the peak in the fourth-order susceptibility. We discuss these next.

B. Fourth order

Two of the fourth-order susceptibilities are shown in Fig. 5. Both χ_{40} and χ_{22} peak at T_c. This was already seen in earlier simulations with $N_t = 4$. Within the resolution of our measurements, we see that the peak in these quantities comes at exactly the same coupling as the peak in χ_L, at both $N_t = 4$ and 6. Like the second order susceptibilities, these too have significant cutoff dependence. χ_{31} is much smaller than either of these susceptibilities and shows no special structure near T_c.

The peak at T_c can be resolved into a single operator expectation value, $(T/V)\langle \mathcal{O}_{22} \rangle$. This expectation value peaks at T_c and falls off rapidly on both sides, as shown in Fig. 6. Therefore it can serve as a good measure of the critical coupling. The expectation value $(T/V)\langle \mathcal{O}_4 \rangle$, on the other hand, shows a crossover near T_c. One could construct yet another measure of the critical coupling from the point of steepest slope of this expectation value, or from its variance, the expectation value $(T/V)\langle \mathcal{O}_{44} \rangle$. This last quantity contributes to eighth order susceptibilities.

Using the fourth and second order quark number susceptibilities, one can form the first two terms of the series expansion of $\chi_{20}(\mu_B)$ [4]. From these coefficients can

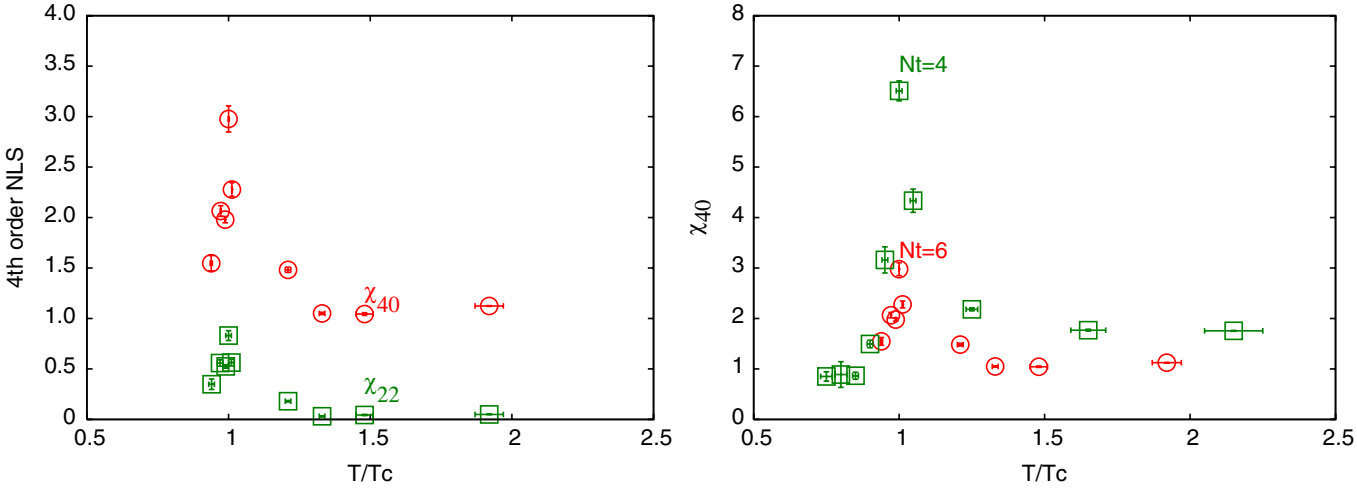

FIG. 5 (color online). Two of the fourth-order susceptibilities on 6×24^3 lattices. Also shown is a comparison of χ_{40} on 6×24^3 and 4×16^3 lattices.

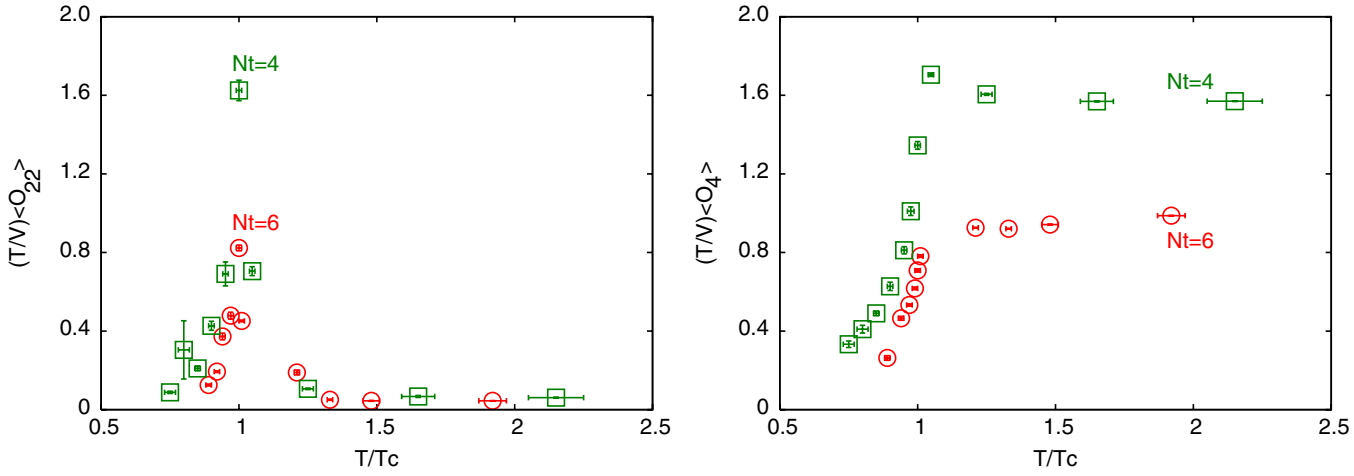

FIG. 6 (color online). The operator expectation values, $(T/V)\langle\mathcal{O}_{22}\rangle$ and $(T/V)\langle\mathcal{O}_4\rangle$ on 6×24^3 (circles) and 4×16^3 (boxes) lattices. The former peaks at T_c whereas the latter exhibits a rapid crossover.

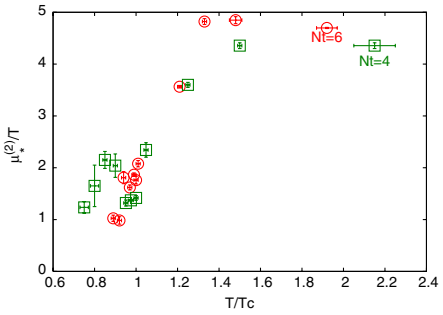

FIG. 7 (color online). The lowest order estimate for the radius of convergence of the Taylor expansion on 6×24^3 (circles) and 4×16^3 (boxes) lattices.

obtain the lowest order estimate of the radius of convergence of this series, $\mu_*^{(n)}$. This is shown as a function of T/T_c in Fig. 7. Note that the large dependence on the lattice spacings seen in each of the susceptibilities almost cancel out in the estimate of the radius of convergence. The radius of convergence has smaller dependence on the lattice spacing.

C. Sixth order

The sixth order NLS is shown in Fig. 8. It has been pointed out earlier that χ_{20} has the form of a rounded step function, and that successively higher order NLS have the form of rounded derivatives of the step function [15]. For example, the fourth-order NLS has a peak. The sixth order NLS changes sign near T_c and has a maximum and a minimum flanking the zero. This behavior is clearly visible in Fig. 8. This peculiar structure comes from the behavior of the expectation value $\langle\mathcal{O}_{222}\rangle$, also shown in Fig. 8. Note that the measurement of $\langle\mathcal{O}_{222}\rangle$ is noisier than that of $\langle\mathcal{O}_{22}\rangle$.

The quark-line connected operator expectation value at this order is $\langle\mathcal{O}_6\rangle$. This is shown in Fig. 9. Note that this has interesting structure below T_c and that the structure is seen

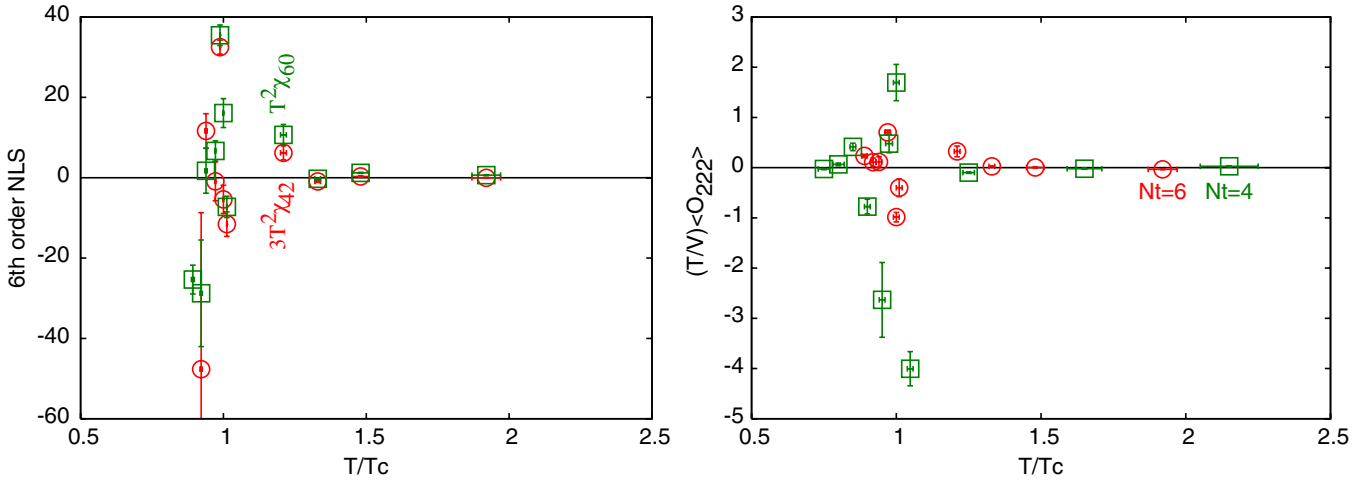

FIG. 8 (color online). Two of the sixth order susceptibilities on 6×24^3 lattices. Also shown is the expectation value which determines the shape of both near T_c on 6×24^3 (circles) and 4×16^3 (boxes) lattices.

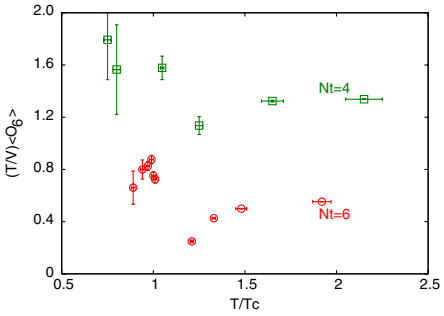

FIG. 9 (color online). The expectation value of the quark-line connected operator which contributes to sixth order NLS on 6×24^3 (circles) and 4×16^3 (boxes) lattices.

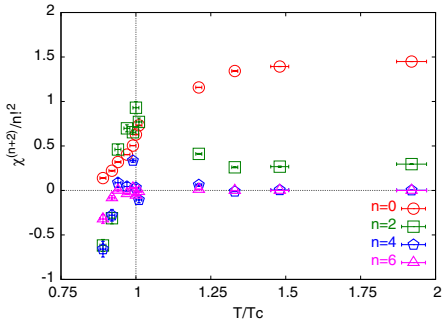

FIG. 11 (color online). Series coefficients in the Taylor expansion of χ_B at various temperatures. Note that the series coefficients have been multiplied by appropriate powers of T to render them dimensionless and by an extra factor of $n!$ to scale them to this figure. There is a small interval in temperature, just below T_c, where all the measured coefficients are positive.

for both $N_t = 4$ and 6. As a result, one cannot use $\langle \mathcal{O}_6 \rangle$ or its variance for determining T_c.

D. Eighth order

The eighth order NLS are fairly noisy below and in the vicinity of T_c. This is partly due to the fact that operators with multiple quark loops, such as $\mathcal{O}_{2222}$, become noisier as the number of loops increases. However, single-loop operators such as $\mathcal{O}_8$ are also not under sufficient control at these lattice volumes. We exhibit the expectation values $\langle \mathcal{O}_8 \rangle$ and $\langle \mathcal{O}_{44} \rangle$ in Fig. 10. Note that there could be structure in the former below T_c, but this is currently obscured by noise. The latter has a single sharp peak at T_c, as argued before, and shows that T_c identified by the peaks in χ_L, χ_{40}, χ_{22}, and $(T/V)\langle \mathcal{O}_{44} \rangle$ are identical within the resolution of our study.

E. Radius of convergence

The radius of convergence of the series expansion can be used to estimate the position of the critical end point of QCD as before. The radius of convergence gives the distance from the origin where the expansion ceases to hold. The corresponding singularity lies at real μ if the coefficients of the series expansion are all positive. In Fig. 11 we show that there is a window in the temperature, just below T_c, in which all the measured coefficients are positive (see also Table III). Interestingly, at all lower temperatures, the coefficients except $\chi^{(2)}$ turn negative. The slopes indicate that the change from negative to positive values may occur at different temperatures for different coefficients.

In the window of temperature where the critical point can be found, we see that only at one of the temperatures in our scan are our estimators of the radius of convergence independent of the method and order (see Fig. 12). At the same temperature we also found that the finite-size effects are in accordance with our expectations: at the smallest volumes the estimators of the radius of convergence increase with order, becoming flat only on the largest volume

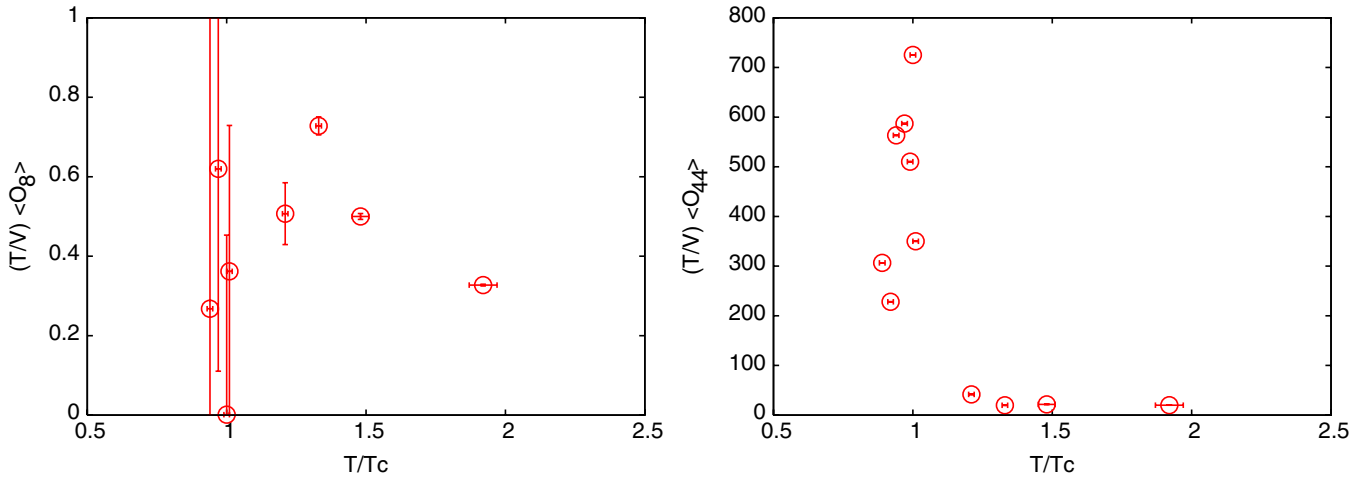

FIG. 10 (color online). Two of the operators which contribute to the eighth order NLS. The quark-line connected operator, $\mathcal{O}_8$ is rather noisy. The connected piece of the expectation value of $\mathcal{O}_{44}$ peaks at T_c, as expected, and is the least noisy of all operators contributing at this order.

TABLE III. The Taylor series coefficients at different temperatures on the lattice with $LT = 4$. There is a lot of structure in these coefficients near T_c (see, for example, [4]). The coefficients are strongly correlated, since they are measured on the same configurations, and hence the computation of the ratios (radii of convergence) and their errors are done through a jackknife analysis.

T/T_c	$\chi_B^{(2)}/T^2$	$\chi_B^{(4)}/2!$	$\chi_B^{(6)}T^2/4!$	$\chi_B^{(8)}T^4/6!$
0.89(1)	0.13(3)	−1.2(1)	16(2)	−232(36)
0.92(1)	0.22(4)	−0.6(1)	−7(2)	−61(18)
0.94(1)	0.32(2)	0.9(1)	2(1)	5(11)
0.97(1)	0.40(1)	1.40(8)	1(1)	27(7)
0.99(1)	0.50(1)	1.31(4)	8.0(5)	19(7)
1.00(1)	0.63(4)	1.9(1)	0.7(9)	−40(12)
1.01(1)	0.73(3)	1.54(8)	−2.5(8)	−10(3)
1.21(1)	1.16(1)	0.82(1)	1.5(4)	8(3)
1.33(1)	1.34(1)	0.52(1)	−0.27(7)	−0.9(3)
1.48(3)	1.39(1)	0.53(1)	0.11(3)	−0.06(4)
1.92(5)	1.449(7)	0.59(2)	0.05(2)	0.16(2)

we studied. With these three interlinked pieces of evidence we estimate the location of the end point to be at

$$\frac{T^E}{T_c} = 0.94 \pm 0.01 \quad \text{and} \quad \frac{\mu_B^E}{T^E} = 1.8 \pm 0.1, \qquad (5)$$

with a lattice spacing of $1/6T$ and a renormalized quark mass that corresponds to tuning $m_\pi \simeq 230$ MeV, when the spatial size of the box is $L = 4/T$.

In comparison, with a lattice spacing of $1/4T$ at the same renormalized quark mass and the same spatial volume, it was found that T^E/T_c remained unchanged whereas one had $\mu_B^E/T^E = 1.3 \pm 0.3$. Extrapolation of this result to the thermodynamic limit, $L \to \infty$, on the coarse lattice yielded an estimate $\mu_B^E/T^E = 1.1 \pm 0.1$, which, although statistically compatible with the finite volume result, had a lower mean. It would be interesting to check how much the new estimate of the QCD critical end point is lowered upon taking the thermodynamic limit. However, this extrapolation lies outside the scope of the current work because of the CPU resources needed.

IV. PHYSICS AT FINITE μ

A. Fluctuations and the quark number susceptibility

Baryon number fluctuations, by an amount ΔB from the expectation value in a grand canonical ensemble, have a spectrum

$$P(\Delta B) = \exp\left(-\frac{(\Delta B)^2}{2VT\chi_B}\right), \quad \text{so} \quad \langle(\Delta B)^2\rangle = VT\chi_B. \quad (6)$$

It has been proposed that the susceptibilities be measured in event-to-event fluctuations in heavy-ion collisions [16]. Indeed, the divergence of the width of the spectrum of fluctuations could be one signal for the detection of the QCD critical point in experiments [17]. In view of this, it is interesting to estimate χ_B as a function of μ_B along the critical isotherm.

While the truncated series expansion can be used to estimate the radius of convergence, it cannot be used to extrapolate the susceptibility up to that point. As shown in Fig. 13, the series expansion for $\chi_B(\mu_B, T)/T^2$ taken to orders $n = 2$ and $n = 4$ fail to agree long before the radius of convergence is reached; nor do they show any diver-

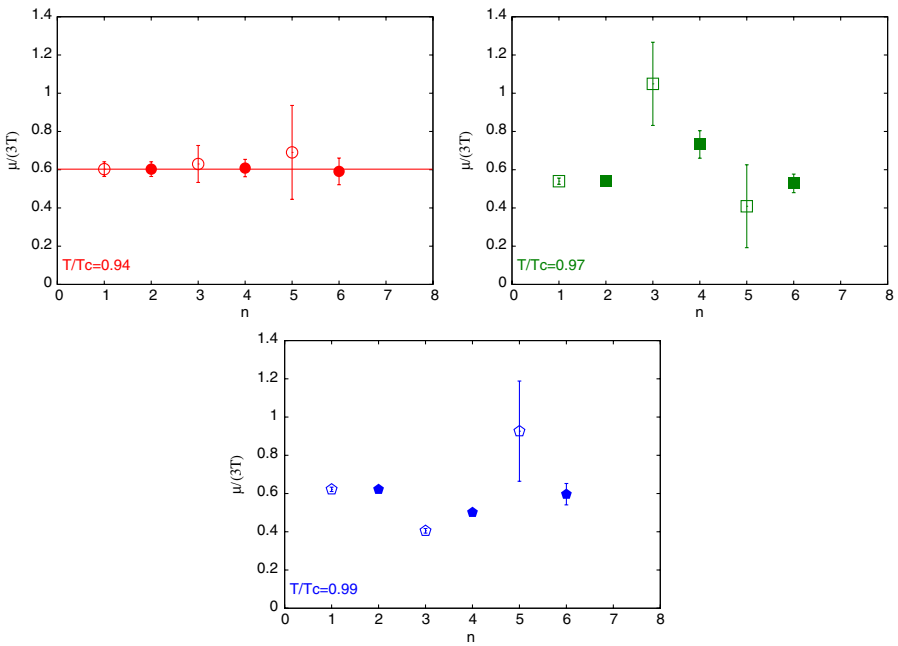

FIG. 12 (color online). Two different estimators of the radius of convergence, $\bar{\mu}_*^{(n)}$ (filled symbols) and $\mu_*^{(n)}$ (open symbols), for different orders, n, on our largest lattice ($LT = 4$) at three different temperatures. Only at one temperature do all the estimators agree.

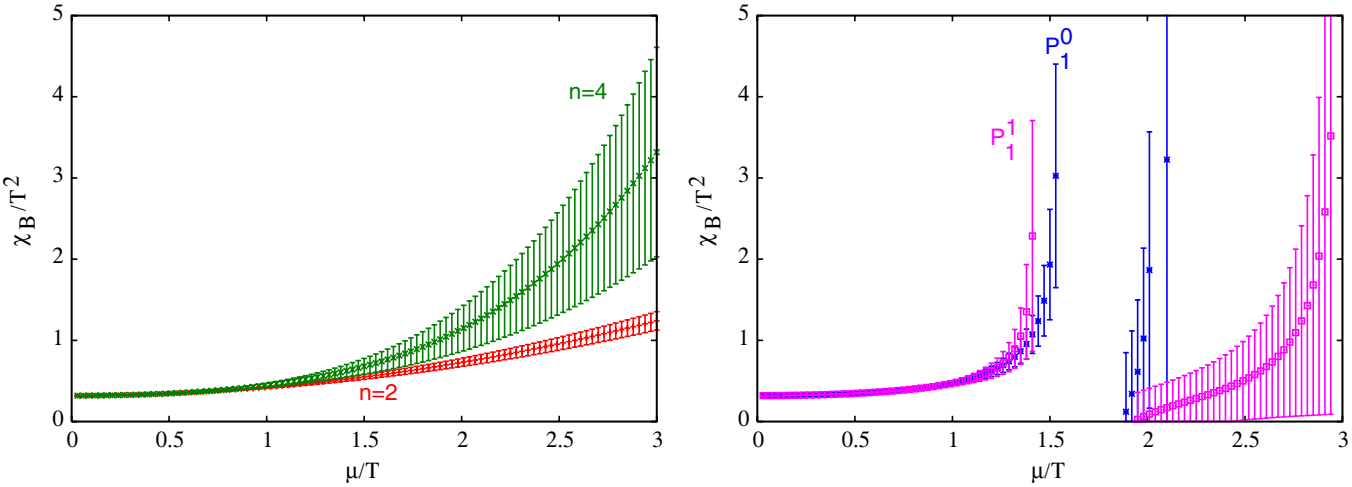

FIG. 13 (color online). $\chi_B(\mu_B, T^E)/(T^E)^2$ obtained through various extrapolations to finite chemical potential. On the left are shown the series expansions to orders $n = 2$ and $n = 4$ (obtained from the fourth and sixth order NLS). The panel on the right shows the extrapolations using Padé approximants.

gence at μ_*. In order to extrapolate the QNS, one must therefore find more robust techniques.

The usual method is to convert the series to a Padé approximant (see [18] for a previous application to QCD). There is extensive literature on the use of these methods when the series expansion is known exactly. In Appendix A we extend this theory to the case relevant to our study, i.e., when the series coefficients are known only through a Monte Carlo procedure, and hence are known with certain errors. The appendix examines error propagation in the Padé approximants and sets out the basic methods to control these errors. For our purposes we use the Padé approximants labeled $P^L_1(\mu_B^2/T^2)$ in the notation in Appendix A.

The Padé approximants $P^0_1(\mu^2/T^2)$ and $P^1_1(\mu^2/T^2)$ are shown in Fig. 13. It is interesting to note that they diverge as μ_B^E/T is approached. While they disagree with the series expansions as the radius of convergence is approached, they remain consistent with each other except very close to the divergence. Note that the errors are large near the divergence. This seems unavoidable, since any error in the coefficients will be magnified near the pole. There are also large errors beyond the pole. It should be possible to control these in future work.

Note that in two-flavor QCD one has $\chi_B = 2\chi_{BQ}$, at all μ_B, as long as the isospin chemical potential remains zero. So there are two independent susceptibilities, χ_B and χ_Q. In terms of the previously computed quantities, they are [19]

$$\chi_B = \tfrac{2}{9}(\chi_{20} + \chi_{11}) \quad \text{and} \quad \chi_Q = \tfrac{2}{81}(5\chi_{20} - 4\chi_{11}). \quad (7)$$

It turns out that χ_{11} remains small within errors even at larger chemical potential, so that the behavior exhibited in Fig. 13 for χ_B is also almost quantitatively correct for χ_Q after an overall normalization by a factor of $5/9$. In particular, the divergence in χ_B is also reflected in χ_Q. This has consequences which we deal with next.

B. Linkage

Earlier works have introduced quantities which measure whether two quantum numbers vary together in thermodynamic fluctuations [19,20]. The most straightforward measure, called the linkage, utilizes diagonal and off-diagonal QNS in the form of the ratio

$$C_{(NM)|N} = C_{(MN)|N} = \frac{\chi_{NM}}{\chi_N}, \quad (8)$$

for any two quantum numbers N and M. The linkage gives the thermal averaged amount of the quantum number M excited per unit N in a thermal fluctuation taking place in the grand canonical ensemble. In two-flavor QCD one may measure the linkage between U and D quantum numbers (conventionally $+1$ for quarks, -1 for antiquarks of the correct flavor, and zero otherwise). Also related is the linkage between the baryon number B and the electrical charge Q.

In Fig. 14 we show the temperature dependence of $C_{(UD)|U}$. At $T = 0$ this quantity should be $-2/3$, since the lightest excitation is a pion, and the two charged pions each give a contribution of -1, whereas the neutral pion gives a contribution of 0. In the high-temperature phase, when the lightest excitations are quark quasiparticles, the linkage should vanish. We see a rapid crossover between these two regimes, with a very small but nonzero value being reached at T_c. We also exhibit the linkage $C_{(BQ)|Q}$. At $T = 0$ this quantity is expected to vanish, since the lightest charged particle, the pion, has no baryon number. In an ideal quark gas, this linkage has value $1/5$. One sees a rapid crossover between these two values in the vicinity of T_c, exactly as for $C_{(UD)|U}$.

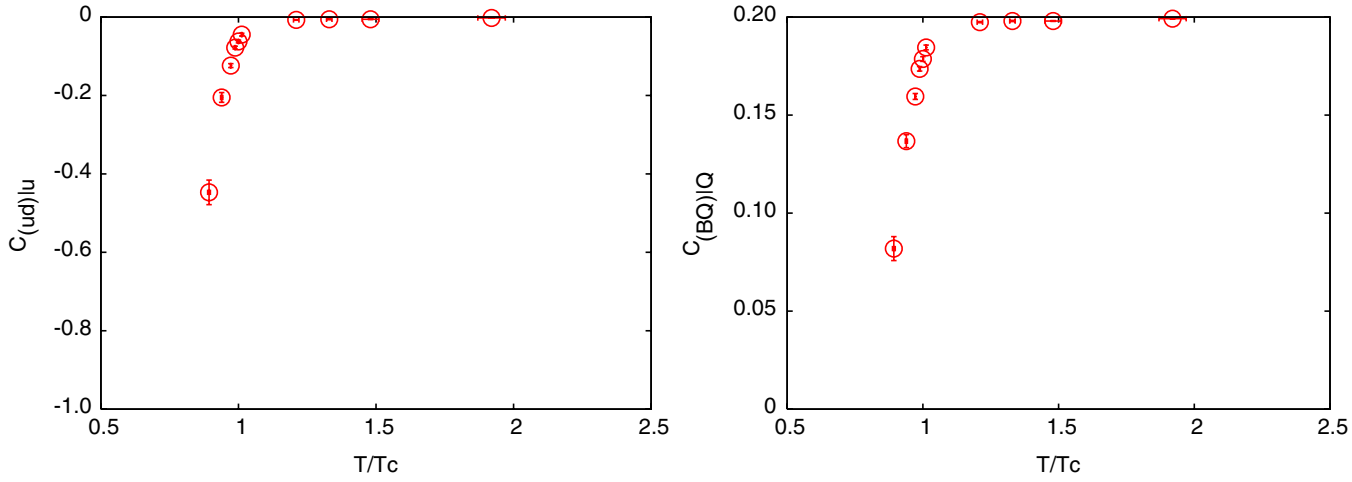

FIG. 14 (color online). The linkages $C_{(UD)|U}$ (left) and $C_{(BQ)|Q}$ (right) as functions of T/T_c at vanishing chemical potentials, as determined on 6×24^3 lattices.

In the chiral limit, i.e., when the quark masses vanish, and a second order phase transition to occur, one would expect that $(T/V)\langle \mathcal{O}_{22} \rangle$ becomes infinitely peaked at T_c. As a result, one expects the diagonal susceptibilities to become infinitely sharp, and the linkages to jump abruptly across the transition. Some part of the rounding in the linkages is therefore due to the fact that the quark masses are finite. However, the rounding of the crossover in the linkages would be a direct demonstration that there is no abrupt change from the hadronic to the quark phase: one may use either description over a small range of temperatures near T_c. This could have implications for the description of hadronization in a fireball, a process which, at the moment, has a very crude description in terms of the Cooper-Frye mechanism [21]. However, a part of the rounding is also due to finite volume effects, and it is hard to disentangle the two in our computation. It would be an interesting future computation to understand quantitatively what part of this slow crossover is a finite volume effect and how much is the effect of a finite quark mass.

Since we have control over the higher order NLS, we can construct a Taylor series expansion for the linkage and examine its behavior at finite chemical potential. For the analytic continuation of the linkage, we perform a jackknife analysis. In each jackknife bin the Padé approximant is evaluated at the chemical potential of interest. The mean of these values is used as the estimator for the continuation, and the 68% interval, evaluated nonparametrically, is quoted as the error bound. The results are shown in Fig. 15 for several different temperatures.

At the highest temperature, i.e. $T/T_c \simeq 2$, the linkage $C_{(UD)|U}$ is close to zero at $\mu_B = 0$ and remains zero for $\mu_B/T \simeq 1$. At temperatures below T_c, the linkage is nonzero at $\mu_B = 0$ but evolves smoothly with the chemical potential. For $T > T^E$ we find a smooth increase with μ_B, the linkage decreasing with larger μ_B. This illustrates the important point that a finite radius of convergence for one susceptibility does not imply divergences in other quantities.

Interestingly, the linkage $C_{(BQ)|Q}$ seems to fall marginally with increasing μ_B. This mild effect can be traced to the fact that the fourth-order coefficient in the Taylor expansion of this linkage is small and negative. This results in a fall at large μ_B. It would be useful to check whether this persists at larger volumes, and whether higher order terms in the expansion turn this around and cause the linkage to increase. An interesting alternative possibility is that the fall in $C_{(BQ)|Q}$ is physical, as is the rise in

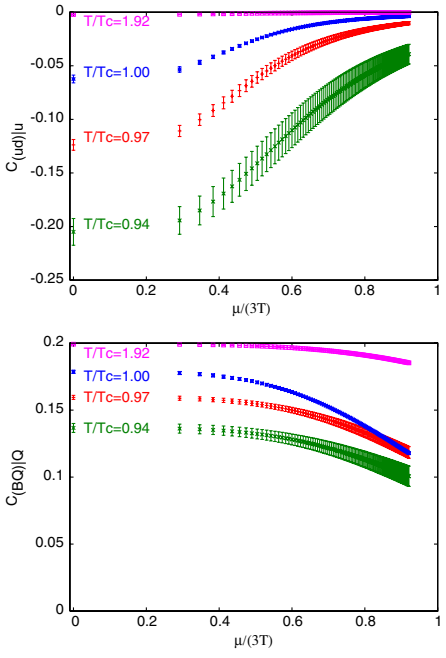

FIG. 15 (color online). The linkages $C_{(UD)|U}$ (left) and $C_{(BQ)|Q}$ (right) as functions of μ/T, as evaluated on 6×24^3 lattices, at four different temperatures.

$C_{(UD)|U}$, and the two together imply the existence of a phase analogous to the quarkyonic phase at large N_c [22]. It is therefore of interest to check these results further. Unfortunately, both checks require massive investment of CPU resources, but are interesting enough that we hope to return to this soon.

V. SUMMARY

We have examined QCD with two flavors of dynamical staggered quarks at finite temperature with lattice spacing $a = 1/6T$ and bare quark masses tuned to $m/T_c = 0.1$. This quark mass is expected to correspond to $m_\pi/m_\rho = 0.3$, and hence our new results are directly comparable to the older results which were obtained on a coarser lattice with $a = 1/4T$ [4]. Our simulations were performed on lattices with size $LT \leq 4$, where L is the spatial size of the box. We used the R-algorithm with a step size in MD time units of 0.01. We have checked that decreasing this by an order of magnitude to 0.001 does not change thermodynamic results (see Table II). Similarly, we have checked that the physics results remain unchanged when the trajectory length is changed.

We identified the crossover at vanishing chemical potential through the Polyakov loop susceptibility χ_L (see Fig. 2) and then cross checked this through two measures related to the QNS. One is the peaking of χ_{40} and χ_{22} (see Fig. 5) which is related to the "inflection point" of the QNS. The other is the peaking of the operator $(T/V)\langle \mathcal{O}_{44}\rangle$, (see Fig. 10) which is related to a similar inflection point in $(T/V)\langle \mathcal{O}_4\rangle$. These measures are consistent with each other within the accuracy of our computations. The scale setting using this identification of the crossover is consistent with the earlier scale setting using coarser lattice spacing [4].

We presented results for the NLS up to eighth order. There are clear lattice spacing effects, as expected. These are roughly consistent with earlier determinations of some of these quantities in quenched theory. While the lattice spacing artifacts for the NLS are very large, sometimes as much as 100%, the effect on the radius of convergence is much smaller (see Fig. 7). Our estimate of the critical point of QCD is based on this radius of convergence. The critical point occurs when the radius of convergence identifies a singularity on the real axis, through the fact that the series coefficients are all positive. Caveats on this are presented in the introduction. Our estimate of the critical point using finite volume data is [see Eq. (5)]

$$\frac{T^E}{T_c} = 0.94 \pm 0.01 \quad \text{and} \quad \frac{\mu_B^E}{T^E} = 1.8 \pm 0.1.$$

This should be compared with our earlier estimate on the same lattice volume and the same renormalized quark mass which gave $\mu_B^E/T^E = 1.3 \pm 0.3$. This is a change of about 26%, and is statistically significant. Extension of our results to larger volumes is outside the scope of this work. In simulations with $a = 1/4T$, the estimate of μ_B^E dropped by about 16% on extrapolating to infinite volume.

The series expansion is a good tool for extracting the radius of convergence, and, through it, the critical point. However, as we show in Fig. 13, it is a bad tool to extrapolate physical results to high μ_B/T. Padé approximants adjusted to give the same series expansion seem to perform better, even after taking into account the propagation of statistical errors. One sees the divergence of the susceptibility at the critical end point, something that the series expansion misses altogether.

We also examined the linkages $C_{(UD)|U}$ and $C_{(BQ)|Q}$ (see Fig. 14). At vanishing chemical potential they show a rapid crossover from the values expected in the hadronic phase to those expected for the nearly ideal quarks. The rounding of this transition is closely related to the question of how sharp the hadronization transition can be in heavy-ion collisions. A discussion of the issue was presented in Sec. IV B.

The measurements of the linkages were extended to finite chemical potential using Padé approximants. Unlike the QNS, they evolve smoothly through the critical point. Interestingly, on isotherms below T_c, with increasing μ_B, the linkage between U and D quantum numbers changes towards the ideal quark gas, whereas the linkage between B and Q changes away from the quark gas. This could indicate the presence of a quarkyonic phase of QCD matter, although technicalities need to be sorted out before one can establish this.

The computations were performed over the last two years on the Cray X1 of the Indian Lattice Gauge Theory Initiative (ILGTI) at TIFR. We thank Ajay Salve for single-handedly taking care of the machine during this extended period.

APPENDIX: PADÉ APPROXIMANTS

We follow Baker's definition [9] of a Padé approximant [23,24]. The series expansion

$$f_N(x) = c_0 + c_1 x + \cdots c_N x^N + \mathcal{O}(x^{N+1}) \tag{A1}$$

evaluated to order N can be used to define the Padé approximant of order L/M,

$$\begin{aligned} P_M^L[f_N(x)] &= \frac{A_M^L(x)}{B_M^L(x)}, \qquad B_M^L(0) = 1, \\ B_M^L(x) f_N(x) - A_M^L(x) &= \mathcal{O}(x^{L+M+1}), \end{aligned} \tag{A2}$$

where $A_M^L(x)$ and $B_M^L(x)$ are polynomials in x or order up to L and M, respectively. From the matching condition it follows that $L + M \leq N$. Introduce the notation—

$$\begin{aligned} A_M^L(x) &= a_0 + a_1 x + \cdots + a_L x^L, \\ B_M^L(x) &= 1 + b_1 x + \cdots + b_M x^M. \end{aligned} \tag{A3}$$

Then, writing out the matching condition order by order,

one obtains the Padé approximants by solving first for the denominator

$$\begin{pmatrix} c_{L-M+1} & c_{L-M+2} & \cdots & c_L \\ c_{L-M+2} & c_{L-M+3} & \cdots & c_{L+1} \\ \vdots & \vdots & & \vdots \\ c_L & c_{L+1} & \cdots & c_{L+M-1} \end{pmatrix} \begin{pmatrix} b_M \\ b_{M-1} \\ \vdots \\ b_1 \end{pmatrix} = -\begin{pmatrix} c_{L+1} \\ c_{L+2} \\ \vdots \\ c_{L+M} \end{pmatrix}, \tag{A4}$$

(with the convention that $c_j = 0$ for $j < 0$) and then for the numerator

$$\begin{aligned} a_0 &= c_0, \\ a_1 &= c_1 + b_1 c_0, \\ &\vdots \\ a_L &= c_L + \sum_{i=1}^{\min(L,M)} b_i c_{L-i}. \end{aligned} \tag{A5}$$

The practical importance of Padé approximants arises from the fact that if the series f_N has a radius of convergence R as $N \to \infty$, then the series expansion is reliable only for $x < R$, whereas the Padé approximants can be used for analytic continuation beyond this. Much of the standard theory of Padé approximants deals with the cases when the coefficient matrix in Eq. (A4) has a vanishing determinant, and the information which can then be extracted.

Here we concentrate on a different problem—that of controlling errors when the series coefficients are obtained by a Monte Carlo program, and hence have a given statistical distribution. We found no discussion of this in the literature, although it is likely that sporadic attempts to answer related questions have been made in the past. These questions become important now that new developments in QCD at finite chemical potential lead us to analyze series coefficients obtained in a Monte Carlo process.

When the Padé coefficients are well defined, the joint probability distribution of the series coefficients can be transformed into that of the coefficients of the Padé approximant using the usual Jacobian formula—

$$\begin{aligned} &\mathcal{P}_M^L(a_0, a_1, \cdots, a_L, b_1, b_2, \cdots, b_M) \\ &\quad = \mathcal{P}(c_0, c_1, \cdots, c_{L+M}) J, \\ &\text{where } J = \frac{\partial(a_0, a_1, \cdots, a_L, b_1, b_2, \cdots, b_M)}{\partial(c_0, c_1, \cdots, c_{L+M})}. \end{aligned} \tag{A6}$$

Take the example of P_1^0, where $a_0 = c_0$ and $b_1 = c_1/c_0$, so that $J = a_0$. Assume that c_0 and c_1 are drawn from independent Gaussian distributions of unit mean—

$$\mathcal{P}_1^0(c_0, c_1) = \frac{1}{2\pi\sigma_0\sigma_1} \exp\left[-\frac{1}{2}\left\{ \frac{(c_0-1)^2}{2\sigma_0^2} + \frac{(c_1-1)^2}{2\sigma_1^2} \right\} \right]. \tag{A7}$$

Then the joint distribution of the Padé coefficients can be written down. The marginal distribution of the Padé coefficient b_1, being the ratio of two Gaussian distributed numbers, is well known [25] and given by

$$\begin{aligned} &\mathcal{P}_1^0(b_1) = \mathrm{e}^{-\mu(b_1)} \frac{2 + \sqrt{2\pi}\lambda(b_1)}{2\pi\sigma_0\sigma_1\nu^2(b_1)}, \\ &\text{where } \nu^2 = \frac{1}{\sigma_0^2} + \frac{b_1^2}{\sigma_1^2}, \\ &\qquad \lambda = \frac{1}{\nu}\left(\frac{1}{\sigma_0^2} + \frac{b_1}{\sigma_1^2} \right), \qquad \mu = \left(\frac{1}{\sigma_0^2} + \frac{1}{\sigma_1^2} \right) - \frac{\lambda^2}{4}. \end{aligned} \tag{A8}$$

Note that $\lambda(\pm\infty) = 1/\sigma_1^2$, and hence $\mu(\pm\infty)$ is a finite number which depends only on $\sigma_{0,1}$. As a result, the marginal distribution of b_1 is not exponentially damped at infinity. The power-law damping comes from the factor $1/\nu^2 \simeq 1/b_1^2$. Clearly this distribution has a well-defined expectation value for b_1, but the variance and higher cumulants do not exist. Thus, statistical measurements of b_1 are not subject to the central limit theorem.

A similar phenomenon occurs with any P_1^L. Assume that the series coefficients are statistically independent and drawn from a Gaussian of unit mean, then the probability distribution of the Padé coefficients can be written as

$$\mathcal{P}_1^L(a_0, a_1, \cdots, a_L, b_1) = \left(\prod_{i=0}^{L+1} \frac{1}{\sqrt{2\pi\sigma_i}} \right) J \exp\left(-\frac{\mathcal{Q}}{2} \right), \tag{A9}$$

where J is the Jacobian of the transformation given by $c_i = \sum_{j \le i} a_{i-j}(-b_1)^j$ for $i \le L$ and $c_{L+1} = c_L b_1$, and $\mathcal{Q}$ is a quadratic form obtained by transforming the arguments of the Gaussians.

The Jacobian of this transformation is

$$J_L = \begin{vmatrix} 1 & 0 & 0 & \cdots & 0 & 0 \\ -b_1 & 1 & 0 & \cdots & 0 & c_1'(b_1) \\ (-b_1)^2 & -b_1 & 1 & \cdots & 0 & c_2'(b_1) \\ \vdots & \vdots & \vdots & & \vdots & \vdots \\ (-b_1)^L & (-b_1)^{L-1} & (-b_1)^{L-2} & \cdots & 1 & c_L'(b_1) \\ b_1(-b_1)^L & b_1(-b_1)^{L-1} & b_1(-b_1)^{L-2} & \cdots & b_1 & c_{L+1}'(b_1) \end{vmatrix}, \tag{A10}$$

where $c_i'(b_1)$ is the derivative of c_i with respect to b_1. Multiplying the second row from the bottom by b_1 and subtracting that from the last row gives

$$J_L = \begin{vmatrix} 1 & 0 & 0 & \cdots & 0 & 0 \\ -b_1 & 1 & 0 & \cdots & 0 & c_1' \\ (-b_1)^2 & -b_1 & 1 & \cdots & 0 & c_2' \\ \vdots & \vdots & \vdots & & \vdots & \vdots \\ (-b_1)^L & (-b_1)^{L-1} & (-b_1)^{L-2} & \cdots & 1 & c_L' \\ 0 & 0 & 0 & \cdots & 0 & c_L \end{vmatrix}$$
$$= c_L = \sum_{i=1}^{L} a_{L-i} b_1^i, \tag{A11}$$

where we have used the relation $c_{L+1} = b_1 c_L$ to write $c_{L+1}' - b_1 c_L' = c_L$.

The quadratic form in the argument of the exponent can be manipulated into a particularly useful form by completing the squares—

$$\mathcal{Q} \equiv \sum_{i=1}^{L+1} \frac{(c_i - 1)^2}{\sigma_i^2} = \mathbf{a}^T Q \mathbf{a} + 2\mathbf{b}^T \mathbf{a} + \sum_{i=1}^{L+1} \frac{1}{\sigma_i^2}$$
$$= (\mathbf{a} - \bar{\mathbf{a}})^T Q (\mathbf{a} - \bar{\mathbf{a}}) + \mu,$$
$$\text{where } \mu = \sum_{i=1}^{L+1} \frac{1}{\sigma_i^2} - \bar{\mathbf{a}}^T Q \bar{\mathbf{a}} \quad \text{and} \quad \bar{\mathbf{a}} = Q^{-1}\mathbf{b}, \tag{A12}$$

where the real symmetric matrix Q and the vector $\mathbf{b}$ can be easily written down. We do this next for the special case when all the σ_i are equal to σ.

Define the sequence of polynomials

$$p_j(b_1) = 1 + b_1^2 + b_1^4 + \cdots + b_1^{2j} = 1 + b_1^2 p_{j-1}(b_1),$$
$$q_j(b_1) = 1 - b_1 + b_1^2 - \cdots + (-b_1)^j = 1 - b_1 q_{j-1}(b_1). \tag{A13}$$

In terms of these, one writes

$$Q = \frac{1}{\sigma^2} \begin{pmatrix} p_{L+1} & -b_1 p_L & b_1^2 p_{L-1} & \cdots \\ -b_1 p_L & p_L & -b_1 p_{L-1} & \cdots \\ b_1^2 p_{L-1} & -b_1 p_{L-1} & p_{L-1} & \cdots \\ \vdots & \vdots & \vdots & \end{pmatrix},$$
$$\mathbf{b} = \begin{pmatrix} q_L \\ q_{L-1} \\ q_{L-2} \\ \cdots \end{pmatrix}. \tag{A14}$$

In order to find the determinant of Q, we do the following row operations—starting from the top, add to each row b_1 times the next row. This reduces the determinant to a lower triangular form

$$\text{Det} Q = \frac{1}{\sigma^2} \begin{vmatrix} 1 & 0 & 0 & \cdots & 0 \\ -b_1 & 1 & 0 & \cdots & 0 \\ b_1^2 & -b_1 & 1 & \cdots & 0 \\ \vdots & \vdots & \vdots & & \vdots \\ (-b_1)^L p_1 & (-b_1)^{L-1} p_1 & (-b_1)^{L-2} p_1 & \cdots & p_1 \end{vmatrix}$$
$$= \frac{p_1(b_1)}{\sigma^2}. \tag{A15}$$

The solution of the equation $Q\bar{\mathbf{a}} = \mathbf{b}$ can be obtained by the same operations. They yield the reduced equation

$$\begin{pmatrix} 1 & 0 & 0 & \cdots & 0 \\ -b_1 & 1 & 0 & \cdots & 0 \\ b_1^2 & -b_1 & 1 & \cdots & 0 \\ \vdots & \vdots & \vdots & & \vdots \\ (-b_1)^L p_1 & (-b_1)^{L-1} p_1 & (-b_1)^{L-2} p_1 & \cdots & p_1 \end{pmatrix} \bar{\mathbf{a}}$$
$$= \sigma^2 \begin{pmatrix} 1 \\ 1 \\ 1 \\ \vdots \\ 1 \end{pmatrix}, \tag{A16}$$

where we have used the relation $q_i(x) = 1 - x q_{i-1}(x)$, to reduce the vector $\mathbf{b}$. This gives

$$\bar{\mathbf{a}} = \sigma^2 \begin{pmatrix} 1 \\ 1+b_1 \\ 1+b_1 \\ \vdots \\ 1+b_1 \\ \frac{1}{1+b_1^2}+b_1 \end{pmatrix}. \tag{A17}$$

Finally,

$$\mu = \frac{L+1}{\sigma^2} - \mathbf{b}^T\bar{\mathbf{a}} = \frac{L+1}{\sigma^2} - \sum_{i=1}^{L}[q_i(b_1) + b_1 q_{i-1}(b_1)] - \frac{1}{1+b_1^2}. \tag{A18}$$

Clearly, μ remains finite in the limit $b_1 \to \pm\infty$, so that $\exp(-\mu/2)$ does not damp the marginal distribution of b_1. In fact, that damping comes from the factor of $1/\mathrm{Det}Q = 1/(1+b_1^2)$. As a result, b_1 has a well-defined mean but its variance is undetermined. Thus, estimators of b_1 evade the central limit theorem.

Nevertheless, the situation is pretty well under control. The appropriate question to ask of a distribution such as that in Eq. (A9) in the context of parameter estimation is not the value of the variance, but an appropriate measure of the variation in the estimate. One could quote the width at half maximum, or the limits such that 68% of the probability lies within these limits. Along with this one asks, if we make N measurements of b_1 then how does such a measure of variation change with N.

A numerical investigation shows that when $\sigma_0 = \sigma_1 = 1$, the modal value is $b = 0.345\,897$. Since the distribution is skew, the modal value and the mean are different. The full width at half maximum is contained in $-0.3485 \le b_1 \le 1.266\,41$, and this range contains 56.1% of the integral. The 68% probability interval is $-0.575 \le b_1 \le 1.38$. Either of these ranges can be quoted as an estimate of the error in the modal value.

To answer the question about the distribution of means, we use the characteristic function. If $f(x)$ is the distribution of x, then the Fourier transform $\tilde{f}(x)$ is called the characteristic function. Since $f(x)$ is non-negative and integrable, being a probability distribution, it is also square integrable, so that the characteristic function exists. The characteristic function of the mean of N numbers, μ_N, is

$$\chi_N(\omega) = \int d\mu_N \exp(i\omega\mu_N) \int\Big[\prod_{j=1}^{N} dx_i f(x_i)\Big] \times \delta\Big(\sum_{j=1}^{N} dx_i - N\mu_N\Big) = \tilde{f}^N\Big(\frac{\omega}{N}\Big). \tag{A19}$$

Fourier transforming this gives the distribution of μ_N. While this general method remains valid for the distributions $\mathcal{P}_1^L$ above, it does not seem possible to perform the Fourier transformations in closed form. So, instead of writing down an impenetrable formula for the distribution of means, we investigate useful subsidiary questions.

Define the skew of a distribution by

$$\mathcal{S} = \frac{x_m}{\langle x\rangle} - 1, \tag{A20}$$

where x_m denotes the modal (most probable) value and $\langle x\rangle$ is the mean. The skew is nonzero for every skewed distribution, being positive if the distribution is skewed to the left and negative otherwise. For the distribution $\mathcal{P}_1^0$, we found $\mathcal{S} = 1.3\cdots$. For the distribution of means of N values, $\mathcal{S}$ decreases. A Monte Carlo estimate for $\sigma_0 = \sigma_1 = 1$ indicates that $\mathcal{S} \approx 3.5/\sqrt{N}$. This estimate was obtained using values of N between 1 and 100. A similar result was obtained for a measure of skewness that compares the median and the mean in a manner analogous to Eq. (A20).

At the median of a distribution, the cumulative distribution becomes equal to 0.5. The errors on the median can be defined as the points at which the cumulative distribution is either 0.34 above or below. The distribution of the means of N numbers narrows rapidly, and we find in a Monte Carlo estimate that both these intervals decrease as $1/\sqrt{N}$.

In conclusion, for the estimation of b_1 and confidence limits on the estimate, it matters little that the central limit theorem does not hold. The mean is well defined, and its difference with the mode and median scale with a factor of $1/\sqrt{N}$. The 68% confidence limits also scale as $1/\sqrt{N}$. We therefore quote the mean and 68% confidence limits on it as estimators for the Padé coefficients. These estimators are easy to incorporate into jackknife and bootstrap analyses. In parts of our analysis the estimators of the series coefficients are also not Gaussian distributed; even so, the nonparametric statistical analysis outlined here suffices.

[1] P. Sorensen (STAR Collaboration), Proc. Sci., CPOD2006 (2006) 20; J. T. Mitchell (PHENIX Collaboration), arXiv: nucl-ex/0701079.

[2] A. Barducci *et al.*, Phys. Lett. B **231**, 463 (1989); M. A. Halasz *et al.*, Phys. Rev. D **58**, 096007 (1998); J. Berges and K. Rajagopal, Nucl. Phys. **B538**, 215 (1999).

[3] R. V. Gavai and S. Gupta, Phys. Rev. D **68**, 034506 (2003).

[4] R. V. Gavai and S. Gupta, Phys. Rev. D **71**, 114014 (2005).

[5] C. R. Allton *et al.*, Phys. Rev. D **71**, 054508 (2005).

[6] Z. Fodor and S. Katz, J. High Energy Phys. 03 (2002) 014;

C. R. Allton *et al.*, Phys. Rev. D **66**, 074507 (2002); M.-P. Lombardo and M. d'Elia, Phys. Rev. D **67**, 014505 (2003); Ph. de Forcrand and O. Philipsen, Nucl. Phys. **B642**, 290 (2002); C. R. Allton *et al.*, Phys. Rev. D **68**, 014507 (2003); Z. Fodor and S. Katz, J. High Energy Phys. 04 (2004) 050; Ph. de Forcrand and O. Philipsen, J. High Energy Phys. 01 (2007) 077; C. Bernard *et al.*, Phys. Rev. D **77**, 014503 (2008).

[7] M. A. Stephanov, Phys. Rev. D **73**, 094508 (2006).

[8] S. A. Gottlieb *et al.*, Phys. Rev. Lett. **59**, 2247 (1987).

[9] G. A. Baker and P. Graves-Morris, *Encyclopedia of Mathematics: Padé Approximants* (Addison-Wesley, Reading, MA, 1981), Vol. 13, Part 1.

[10] Y. Aoki *et al.*, Phys. Lett. B **643**, 46 (2006); M. Cheng *et al.*, Phys. Rev. D **74**, 054507 (2006); C. Detar *et al.*, Proc. Sci., LAT2007 (2007) 179.

[11] S. Gottlieb *et al.*, Phys. Rev. Lett. **59**, 1513 (1987).

[12] C. Bernard *et al.*, Phys. Rev. D **45**, 3854 (1992).

[13] R. V. Gavai and S. Gupta, Nucl. Phys. A **785**, 18 (2007).

[14] R. V. Gavai and S. Gupta, Phys. Rev. D **67**, 034501 (2003).

[15] R. V. Gavai and S. Gupta, Phys. Rev. D **72**, 054006 (2005).

[16] M. Asakawa, U. Heinz, and B. Muller, Phys. Rev. Lett. **85**, 2072 (2000); S. Jeon and V. Koch, Phys. Rev. Lett. **85**, 2076 (2000).

[17] M. A. Stephanov, K. Rajagopal, and E. V. Shuryak, Phys. Rev. D **60**, 114028 (1999); M. A. Stephanov, K. Rajagopal, and E. Shuryak, Phys. Rev. Lett. **81**, 4816 (1998); G. S. F. Stephans, J. Phys. G **32**, S447 (2006); P. Sorensen (STAR Collaboration), Proc. Sci., CPOD2006 (2006) 019 [arXiv:nucl-ex/0701028].

[18] M. P. Lombardo, Proc. Sci., LAT2005 (2006) 168 [arXiv: hep-lat/0509181].

[19] R. V. Gavai and S. Gupta, Phys. Rev. D **73**, 014004 (2006).

[20] V. Koch, A. Majumder, and J. Randrup, Phys. Rev. Lett. **95**, 182301 (2005).

[21] F. Cooper and G. Frye, Phys. Rev. D **10**, 186 (1974).

[22] L. McLerran and R. D. Pisarski, Nucl. Phys. A **796**, 83 (2007).

[23] H. Pade, Annales de l'Ecole Normale Superieur **3** (9 Suppl), 3 (1892).

[24] D. S. Gaunt and A. J. Guttmann, *Phase Transitions and Critical Phenomena*, edited by C. Domb and M. S. Green (Academic, London, 1974), Vol. 3, p. 181.

[25] R. C. Geary, J. R. Stat. Soc. **93**, 442 (1930).